TOPOLOGICAL OPTICS

Nonlinear tuning of PT symmetry and non-Hermitian topological states

Shiqi Xia[1]*, Dimitrios Kaltsas[2]*, Daohong Song[1]*, Ioannis Komis[2], Jingjun Xu[1], Alexander Szameit[3], Hrvoje Buljan[1,4]†, Konstantinos G. Makris[2,5]†, Zhigang Chen[1,6]†

Topology, parity-time (PT) symmetry, and nonlinearity are at the origin of many fundamental phenomena in complex systems across the natural sciences, but their mutual interplay remains unexplored. We established a nonlinear non-Hermitian topological platform for active tuning of PT symmetry and topological states. We found that the loss in a topological defect potential in a non-Hermitian photonic lattice can be tuned solely by nonlinearity, enabling the transition between PT-symmetric and non–PT-symmetric regimes and the maneuvering of topological zero modes. The interaction between two apparently antagonistic effects is revealed: the sensitivity close to exceptional points and the robustness of non-Hermitian topological states. Our scheme using single-channel control of global PT symmetry and topology via local nonlinearity may provide opportunities for unconventional light manipulation and device applications.

Although there are numerous distinct phenomena mediated by topology, symmetry, and nonlinearity, a complex system simultaneously exhibiting all these features is hard to find. In 2008, two important concepts—the quantum Hall edge state and parity-time (PT) symmetry—were introduced to photonics (1, 2), leading to the birth of topological photonics (3) and non-Hermitian optics (4), respectively. Topological photonics, the use of topological ideas to control the behavior of light, has been realized in a variety of photonic settings (3, 5–7). PT symmetry in optics, by contrast, is implemented using a complex refractive index and has also provided a plethora of alternative designs for controlling light, aiming toward new types of photonic devices based on non-Hermitian physics (4, 8–10). Combining the two areas is conceptually challenging, but experiments have shown that topological edge states can indeed be observed in non-Hermitian systems (11, 12). Moreover, non-Hermitian characteristics give rise to intriguing topological phenomena such as topological light steering and funneling (13, 14). One striking development relevant to technological applications is the demonstration of topological insulator lasers (15, 16), in which topology and non-Hermiticity naturally coalesce and conspire: Lasing is based on topologically protected

modes, and a laser system is inherently non-Hermitian because gain and loss are present. However, so far, non-Hermitian topological photonics have mainly been restricted to the linear-optics regime, and only recently has it become clear that many intriguing phenomena arise when nonlinearity is taken into account in nonlinear non-Hermitian (NNH) topological systems (17–21).

We demonstrate a scheme for single-channel nonlinear control of a complex system with underlying global dynamics driven by the interplay among topology, non-Hermiticity, and nonlinearity. Our experimental platform is based on photonic Su-Schrieffer-Heeger (SSH) (22, 23) lattices consisting of laser-written continuous ("gain") and sectioned ("loss") waveguides with an interface defect (Fig. 1A), but it applies equally to a broad spectrum of NNH systems that have intensity-dependent gain or loss. The SSH lattices represent a prototypical one-dimensional topological system with chiral symmetry (3), as is widely used for the study of topologically protected quantum states (24), nonlinearity-driven topological effects (21, 25–27), and topological lasing (28), among other things.

It is known that an active linear non-Hermitian PT-symmetric system can be directly mapped onto a system with only loss simply by introducing a global decay factor (equivalent to an offset for the imaginary part described by the gain-loss profile) (4). In such "passive" PT-symmetric systems, non-Hermitian PT phenomena have been demonstrated without using actual material gain (8, 12). Unlike previous implementations of loss, we use a weak continuous-wave (cw) laser to write nonlinear non-Hermitian SSH lattices (NNH-SSHs) in a bulk nonlinear crystal (27), as illustrated in Fig. 1A. The continuous waveguides (red) represent the "gain" ones, whereas the sectioned waveguides can be "lossy" (blue) or "neutral"

(green) depending on the gap size introduced between sections. An NNH-SSH that is realized in the passive PT-symmetric regime may, under the action of self-focusing nonlinearity experienced by a probe beam at the interface, change into a non-PT "gain" system, as self-focusing reduces diffraction loss and leakage in the center waveguide. Likewise, under the action of self-defocusing nonlinearity, it may turn into a non-PT "loss" system, because in this case the nonlinearity enhances the leakage and entails more loss in the waveguide. In this way, nonlinear excitation of a single channel (i.e., the interface waveguide) can locally affect the properties of the whole lattice, leading to transition from PT-symmetric to non–PT-symmetric regimes. Because all three NNH-SSHs ("gain," "loss," and "neutral") can be initially implemented in experiment, our explored platform enables a convenient approach to achieving nonlinearity-induced switching between different non-Hermitian lattices. Interestingly, the Hamiltonians of these NNH-SSHs are inherently related (29), and the underlying connection directly affects corresponding complex eigenvalue spectra across the exceptional point (EP)—a special kind of degeneracy with coalesced eigenvalues and eigenstates unique to non-Hermitian Hamiltonians (30).

Our experimental method to establish the NNH-SSHs is illustrated in Fig. 1B, where the writing beam is either a uniform stripe beam (for writing the "gain" waveguides) or a periodically modulated beam (for writing the sectioned "loss" and "neutral" waveguides). The waveguides are written sideways one by one in a biased photorefractive (SBN:61) crystal (27). In the entire writing process, the bias field is $E_0 = 160$ kV/m, the writing beam has a power of ~200 μW, and the probing beam has a power of ~2.5 μW. [See (29) for other experimental details.] A passive PT-symmetric SSH system requires precise control of loss. To achieve this, we keep the same total number of waveguide sections (with section length l) in each channel (17 sections in the 20-mm-long crystal), but we make the spacing between adjacent sections (i.e., the gap length m) smaller in the "neutral" waveguide than in the "loss" waveguides. A superimposed writing beam pattern is shown in Fig. 1C, consisting of alternating continuous and sectioned stripes relative to the center defect channel. A typical NNH-SSH written this way is shown in Fig. 1D, for which strong and weak coupling correspond to smaller and larger channel separation, respectively. Figure 1E plots the normalized intensity transmission ratio (defined as $y = I_{out}/I_0$, where I_{out} and I_0 are the output intensity of the same probe beam from a sectioned and a continuous waveguide, respectively) as a function of the gap ratio (defined as $x = m/l$, which controls the waveguide loss). As the gap length increases, the loss in the waveguide increases,

[1]MOE Key Laboratory of Weak-Light Nonlinear Photonics, TEDA Applied Physics Institute and School of Physics, Nankai University, Tianjin 300457, China. [2]Department of Physics, University of Crete, Heraklion 71003, Greece. [3]Institut für Physik, Universität Rostock, 18059 Rostock, Germany. [4]Department of Physics, Faculty of Science, University of Zagreb, 10000 Zagreb, Croatia. [5]Institute of Electronic Structure and Laser (IESL)–FORTH, Heraklion 71110, Greece. [6]Department of Physics and Astronomy, San Francisco State University, San Francisco, CA 94132, USA.
*These authors contributed equally to this work.
†Corresponding author. Email: hbuljan@phy.hr (H.B.); makris@physics.uoc.gr (K.G.M.); zgchen@nankai.edu.cn (Z.C.)
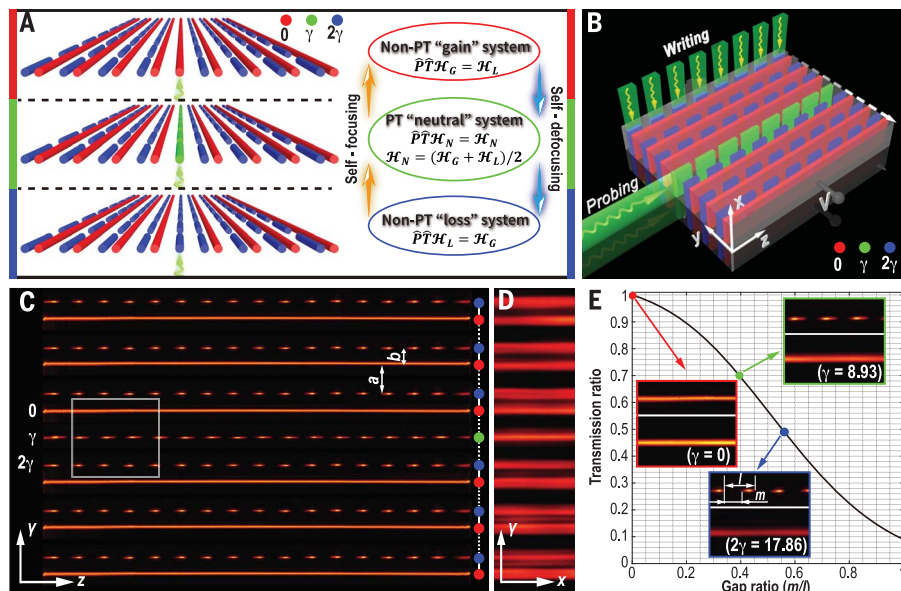
Fig. 1. Experimental realization of NNH-SSHs for nonlinear tuning of PT symmetry and topological states. (**A**) Illustration of a passive PT-symmetric "neutral" SSH lattice (middle) switched to a non-PT "gain" lattice (top) or a non-PT "loss" lattice (bottom) by local nonlinearity at the topological defect. The switching direction can be readily reversed. Red, green, and blue cylinders and dots represent "gain," "neutral," and "loss" lattice sites (γ is the loss coefficient); colored bars denote different stages of the NNH-SSHs. The Hamiltonian relations are illustrated for corresponding active non-Hermitian systems (*29*). (**B**) Schematic for cw-laser writing and probing the lattices. A dashed white arrow marks the writing sequence. (**C**) Side view of the writing beam pattern, where $a = 22.8$ μm and $b = 15.2$ μm represent waveguide spacing for the dimer lattice. (**D**) The written NNH-SSH examined by a broad plane-wave beam. (**E**) Plot of intensity transmission ratio as a function of the gap ratio in a single waveguide obtained from simulation. Insets show side views of a waveguide portion taken from the experiment in (C) at $m/l = 0$ (red), 0.40 (green), and 0.56 (blue), where in each inset a single writing beam is shown at the top and the guided output probe beam at the bottom.

and thus the transmission decreases (Fig. 1E, insets). The loss coefficient γ is determined from the intensity transmission $I_{out} = I_0 \exp(-2\gamma L)$, where $L = 20$ mm corresponds to the crystal length (*29*). This plot serves as the basis for determining the parameters for the writing beams in the experiment. For example, the "gain" waveguide ($\gamma = 0$) corresponds to the red dot at $(x, y) = (0, 1)$, because it is continuous ($m = 0$) and lossless. The "neutral" waveguide, marked by the green dot at $(x, y) = (0.40, 0.70)$, corresponds to a gap ratio of 0.40 and a transmission ratio of 0.70, which yields $\gamma = 8.93$ m^{-1}. From this, we can in turn find the parameters for the "loss" waveguides, marked by the blue dot at $(x, y) = (0.56, 0.49)$, and obtain the desired loss 2γ. The NNH-SSH established with such judiciously introduced losses fulfills the requirement for PT symmetry.

Before presenting the experimental results, we examine theoretically the topological states in a corresponding active PT-symmetric SSH lattice with an interface defect, as illustrated in Fig. 2A. Under the tight-binding approximation, the linear coupled mode equations are

$$-i\frac{\partial}{\partial z}\varphi_n = \beta^*\varphi_n + c_1\varphi_{n-1} + c_2\varphi_{n+1},$$
$$n = 2, 4, \dots \text{ or } -1, -3, \dots \quad (1a)$$

$$-i\frac{\partial}{\partial z}\varphi_n = \beta\varphi_n + c_2\varphi_{n-1} + c_1\varphi_{n+1},$$
$$n = 1, 3, \dots \text{ or } -2, -4, \dots \quad (1b)$$

$$-i\frac{\partial}{\partial z}\varphi_0 = \beta_0\varphi_0 + c_2\varphi_1 + c_2\varphi_{-1}, \; n = 0 \quad (1c)$$

(*11*, *12*), where φ_n denotes the modal amplitude in the nth waveguide, $\beta = \alpha + i\gamma$ (α and γ are the real and imaginary parts of the waveguide potential), c_1 and c_2 are the strong and weak coupling coefficients, and β_0 denotes the potential of the center defect waveguide at $n = 0$. If $\gamma = 0$ for all waveguides, the non-Hermitian SSH collapses to the Hermitian model that supports topologically protected mid-gap (zero-mode) states (*25*). Even when the loss or gain is introduced ($\gamma \neq 0$), the non-Hermitian SSH lattice described above still supports a PT-symmetric topological state, provided that there is no gain or loss at the dimerization defect (*12*)—that is, $\beta_0 = \alpha$, $\gamma_0 = 0$. In our model, we assume that the lattice is terminated at the weak-coupling bond (c_2) such that no edge states are present on either side (*23*). The results are summarized in Fig. 2B, showing how a topological interface state is affected by non-Hermiticity and nonlinearity. The above equa-

tions can be expressed in a matrix form, and the relations between the Hamiltonians $\mathcal{H}_G$, $\mathcal{H}_L$, and $\mathcal{H}_N$ (corresponding to the three lattices) are given in Fig. 1A (*29*).

Our lattices consist of 33 waveguides with $c_1 = 4$, $c_2 = 1$. The linear propagation constant for all waveguides is set as $\alpha = 0$, $\gamma = 1$, except for $n = 0$. In the linear regime, α is the same for all waveguides, and a typical PT-symmetric mid-gap interface state is represented by point A in Fig. 2B. As seen from the top left panel of Fig. 2B, all eigenmodes have only real eigenvalues, because the lattice is in the PT symmetry–unbroken regime (*12*). In the nonlinear regime, the propagation constant is intensity-dependent: $\beta(I) = \alpha(I) + i\gamma(I)$, where I is the intensity of the excitation beam. As such, the eigenvalue of the topological state can be moved away from its initial mid-gap position by the action of the nonlinearity (*25*, *27*). Because a probe beam excites only the center defect channel while it experiences an overall loss in a passive NNH-SSH, it is reasonable to model the system with nonlinearity present only in the defect channel: $\beta_0(I) = \alpha_0(I) + i\gamma_0(I)$. If the nonlinearity only changes the real part of the potential while keeping $\gamma_0 = 0$, the eigenvalue of the zero mode is shifted away from the center of the gap, moving upward (or downward) as a consequence of the self-focusing (or -defocusing) effect to point B (or C) in Fig. 2B. The eigenmode profiles remain as symmetric as that of the mid-gap mode because the lattice overall still preserves the PT symmetry. In contrast, if the nonlinearity also changes the imaginary part of the potential γ_0, PT symmetry is destroyed. This scenario corresponds to results marked by points D and E, where the imaginary part of the eigenvalues is shifted away from the zero-mode position. In this non-PT regime, the eigenmode profiles become asymmetric, as more energy of the modes flows to the "loss" (D) or "gain" (E) waveguides depending on the sign of the nonlinearity. Thus, the observation of nonlinearity-induced asymmetric mode profiles in the NNH-SSHs serves as a signature for the change of the imaginary part of the defect potential, indicating whether PT symmetry is present or not.

With the NNH-SSHs implemented by cw-laser writing (Fig. 1), we experimentally demonstrated this nonlinear tuning of the zero mode by launching a probe beam into the defect channel (Fig. 3, bottom row). Starting from linear propagation (i.e., without the bias field), a symmetric topological interface state (corresponding to point A in Fig. 2B) is observed in the "neutral" lattice (Fig. 3B, second row), which indicates that in this case the NNH-SSH respects the PT symmetry (*12*). However, under the action of a self-defocusing nonlinearity, the probe beam induces anti-guiding so that more

of its energy escapes from the defect channel, equivalently introducing leakage ("loss") to the center waveguide. The NNH-SSH turns into a non–PT-symmetric structure, and the excited mode becomes asymmetric (Fig. 3B, first row) as more light goes to the "loss" waveguide, corresponding to point D in Fig. 2B. In contrast, when a self-focusing nonlinearity is used, it induces self-guiding, such that the diffraction is suppressed, equivalently providing "gain" to the center waveguide. Again, the beam becomes asymmetric but now more light goes to the "gain" waveguide, corresponding to point E in Fig. 2B. Because evidently the change in the real part of the index potential alone does not result in asymmetric modes, our results represent a nonlinearity-induced transition from a PT-symmetric lattice to a non-Hermitian lattice without PT symmetry.

As illustrated in Fig. 1A, the transition can also be reversed by nonlinearity. Such results are shown in Fig. 3A with an initial "gain" NNH-SSH, and in Fig. 3C with an initial "loss" NNH-SSH. In the non-PT "gain" lattice, a probe beam evolves linearly into an asymmetric distribution. Under self-defocusing nonlinearity, a symmetric profile with the characteristic feature of a topological interface state is restored (Fig. 3A, first row), as nonlinearity entails the retrieval of lattice PT symmetry. However, in this case, it cannot be restored with self-focusing nonlinearity, which increases the gain-loss imbalance (Fig. 3A, third row). The scenario corresponding to an inversed transition starting from a non-PT "loss" to a PT-symmetric lattice is shown in Fig. 3C. These results, corroborated by numerical simulations (29), clearly demonstrate nonlinearity-mediated control of PT symmetry and topological states in the NNH-SSHs.

So far, we have shown that local nonlinearity can be used to control the loss in the defect waveguide, thereby affecting the global lattice properties. We now discuss tuning of the NNH-SSHs close to the EPs, where intriguing
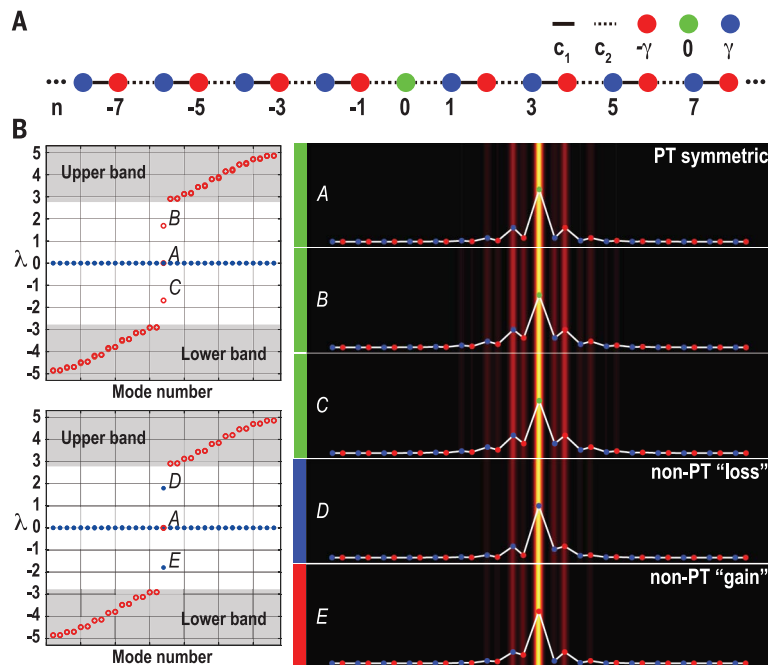

Fig. 2. Calculated non-Hermitian topological interface states tuned by nonlinearity. (**A**) Illustration of an active PT-symmetric SSH with an interface topological defect located at site $n = 0$. Colored dots represent different lattice sites. (**B**) Left: Calculated eigenvalues λ for a finite lattice with 33 sites. Red circles and blue dots denote real and imaginary parts of the eigenvalues, respectively; shaded regions illustrate the band structure of an infinite lattice. Right: The corresponding eigenmode profiles, where the eigenvalues for points A to E are obtained with propagation constants $\beta_0 = 0, 2, -2, 2i$, and $-2i$ while keeping β for all other waveguides unchanged. Color codes for different waveguides are the same as in Fig. 1.
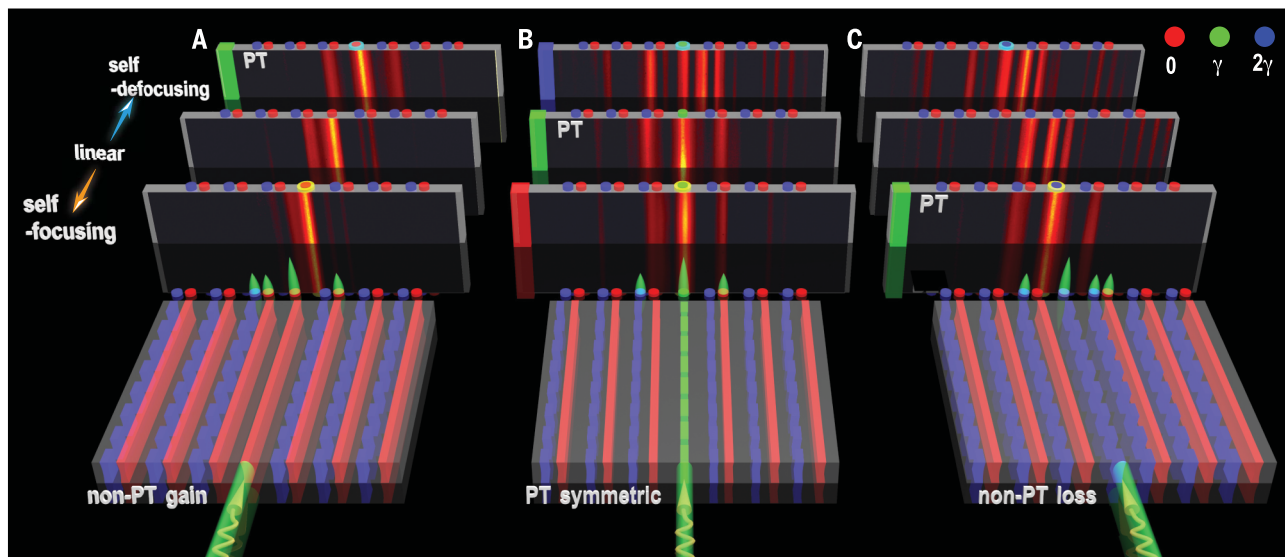

Fig. 3. Demonstration of single-channel nonlinear control of PT symmetry and topological states. (**A** to **C**) Top three rows: Experimental results showing output transverse patterns of a probe beam launched into the defect channel for three distinct cases. The NNH-SSH is fabricated with a "gain" (A), "neutral" (B), or "loss" (C) interface waveguide. Bottom row: Schematic of the excitation beam and the corresponding linear mode profile. In the linear regime, only the "neutral" lattice (B) initially has PT symmetry. In (A) and (C), the lattice is non–PT-symmetric, but PT symmetry and topological states are restored under the action of nonlinearity.

properties are expected for non-Hermitian systems (*30–32*). To this end, in our model we considered a scan through the EPs by changing the global gain or loss amplitude; our findings are summarized in Fig. 4, A and B. For the three lattices defined earlier, we kept the potential of the central defect waveguide fixed (as set by the nonlinearity in our experiment) and varied the gain/loss ratio for all other waveguides. The complex eigenvalue spectra λ_n exhibit a markedly different bifurcation feature: Before reaching the EP of the PT-symmetric lattice, which has only real eigenvalues, they come in complex conjugate pairs (with different ranges of imaginary magnitudes) for the other two lattices; after a certain value of gain/loss ratio beyond the pertinent EP, all three lattices exhibit the same range of imaginary eigenvalues determined by the bulk modes of the lattices (Fig. 4A). This is a direct outcome of the inherent connection between the Hamiltonians (*29*). At the EP, the bandgap closes and the topologically protected mode becomes extended, which suggests that a phase transition should have taken place. This can be clearly seen from the sharp drop of the transmitted intensity through the defect channel after a long propagation distance in all three lattices (Fig. 4B): The cusp followed by a continuous rise of the intensity indicates the presence of an EP in each lattice. Moreover, with the nonlinear tuning illustrated in Fig. 4A, our scheme can give rise to the birth or death of EPs for the NNH-SSHs (*29*), which merits further investigation.

A direct outcome of the topological nature of the SSH model is the robustness of zero modes to perturbation in the off-diagonal of the Hamiltonian. One may wonder which of the two opposite tendencies will prevail: the sensitivity or the robustness, especially when close to the EP (*30–32*). We theoretically address this question in Fig. 4C, where the defect mode eigenvalues are plotted on the complex plane for various values of defect potential but the gain/loss ratio is fixed for the rest of the lattice. We examine the robustness of the defect mode to off-diagonal perturbations (15% on the coupling coefficients) that respect the lattice chiral symmetry. Strictly speaking, only the PT-symmetric lattice supports the exact zero mode with complete topological robustness. Once the eigenvalue of the defect mode is driven away from the origin in the complex plane, topological protection is gradually lost. Interestingly, this loss of protection is not "isotropic" (in a sense that the instability of the defect mode grows in a preferred direction in the complex spectra), but is enhanced when the parameters are tuned close to the EP.

Topology and PT symmetry typically describe the global properties of a system, whereas most optical nonlinearities are local. Therefore, their
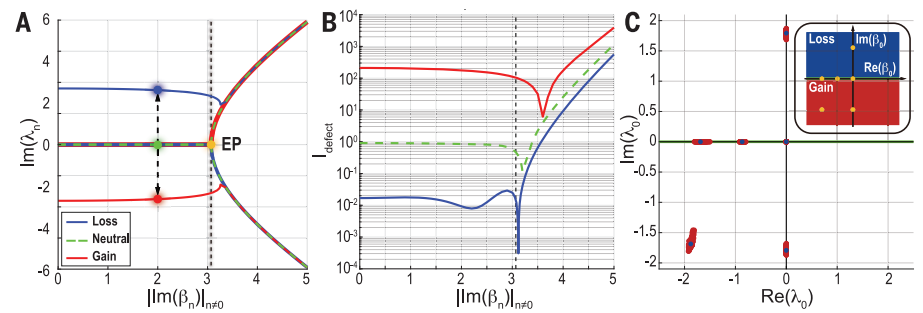
interplay in some sense is a manifestation of the interplay of local and global characteristics. It is natural to ask: Is there a general theory for the NNH PT-symmetric systems driven by nonlinearity (*29*)? Beyond that, there are many fundamental questions yet to answer. For instance, how can one characterize topological invariants for finite NNH-SSHs driven by nonlinearity, given that the concept developed for linear Hermitian systems is not equally applicable? More intriguingly, can nonlinearity induce crossing or encircling of the EP (*31, 32*) in order to control the dynamics of topological modes? Is it possible to tune the bandgap structures and remotely control the power flow at a target destination far from a topological defect in NNH systems? How would local nonlinearity affect overall topological features and classifications of symmetry and topology (*33*)? We envisage that nonlinear control may play a unique role in integrating these concepts to harness complex systems beyond photonics, including but not limited to acoustics, plasmonics, polaritonics, and ultracold atoms.

Fig. 4. Theoretical analysis of complex spectra around the EP and zero-mode robustness. (**A**) The range of the imaginary part of the complex eigenvalues (maximal/minimal magnitudes) as a function of the global gain-loss amplitude for three NNH-SSHs. The EP is marked for the "neutral" PT-symmetric lattice. Colored dots before the EP correspond to experimental gain/loss parameters ($\beta_0 = 2i$, 0, $-2i$) at the defect waveguide; they can be switched via nonlinearity, as indicated by the dashed arrow. Other lattice parameters are the same as for Fig. 2. (**B**) Plot of defect-channel intensity in the NNH-SSHs tuned across the EP under the same initial conditions. (**C**) Sensitivity of defect-mode eigenvalues to the perturbation on coupling coefficients when $|Im(\beta_n)|_{n\neq0}$ is fixed to 1. Red dots denote the eigenvalue fluctuation for 100 realizations of added perturbation; the blue dots correspond to the initial defect eigenvalue. The inset depicts corresponding values of the central defect potential β_0 on the complex plane. Notice the robustness of the exact zero mode at the origin.

REFERENCES AND NOTES

1. F. D. Haldane, S. Raghu, *Phys. Rev. Lett.* **100**, 013904 (2008).
2. K. G. Makris, R. El-Ganainy, D. N. Christodoulides, Z. H. Musslimani, *Phys. Rev. Lett.* **100**, 103904 (2008).
3. T. Ozawa et al., *Rev. Mod. Phys.* **91**, 015006 (2019).
4. R. El-Ganainy et al., *Nat. Phys.* **14**, 11–19 (2018).
5. Z. Wang, Y. Chong, J. D. Joannopoulos, M. Soljačić, *Nature* **461**, 772–775 (2009).
6. M. C. Rechtsman et al., *Nature* **496**, 196–200 (2013).
7. M. Hafezi, S. Mittal, J. Fan, A. Migdall, J. M. Taylor, *Nat. Photonics* **7**, 1001–1005 (2013).
8. A. Guo et al., *Phys. Rev. Lett.* **103**, 093902 (2009).
9. C. E. Rüter et al., *Nat. Phys.* **6**, 192–195 (2010).
10. A. Regensburger et al., *Nature* **488**, 167–171 (2012).
11. C. Poli, M. Bellec, U. Kuhl, F. Mortessagne, H. Schomerus, *Nat. Commun.* **6**, 6710 (2015).
12. S. Weimann et al., *Nat. Mater.* **16**, 433–438 (2017).
13. H. Zhao et al., *Science* **365**, 1163–1166 (2019).
14. S. Weidemann et al., *Science* **368**, 311–314 (2020).
15. M. A. Bandres et al., *Science* **359**, eaar4005 (2018).
16. G. Harari et al., *Science* **359**, eaar4003 (2018).
17. M. Wimmer et al., *Nat. Commun.* **6**, 7782 (2015).
18. Y. Lumer, Y. Plotnik, M. C. Rechtsman, M. Segev, *Phys. Rev. Lett.* **111**, 243905 (2013).
19. S. Mukherjee, M. C. Rechtsman, *Science* **368**, 856–859 (2020).
20. L. J. Maczewsky et al., *Science* **370**, 701–704 (2020).
21. D. Smirnova, D. Leykam, Y. Chong, Y. Kivshar, *Appl. Phys. Rev.* **7**, 021306 (2020).
22. W. P. Su, J. R. Schrieffer, A. J. Heeger, *Phys. Rev. Lett.* **42**, 1698–1701 (1979).
23. N. Malkova, I. Hromada, X. Wang, G. Bryant, Z. Chen, *Opt. Lett.* **34**, 1633–1635 (2009).
24. A. Blanco-Redondo, B. Bell, D. Oren, B. J. Eggleton, M. Segev, *Science* **362**, 568–571 (2018).
25. N. Malkova, I. Hromada, X. Wang, G. Bryant, Z. Chen, *Phys. Rev. A* **80**, 043806 (2009).
26. Y. Hadad, A. B. Khanikaev, A. Alù, *Phys. Rev. B* **93**, 155112 (2016).
27. S. Xia et al., *Light Sci. Appl.* **9**, 147 (2020).
28. P. St-Jean et al., *Nat. Photonics* **11**, 651–656 (2017).
29. See supplementary materials.
30. Ş. K. Özdemir, S. Rotter, F. Nori, L. Yang, *Nat. Mater.* **18**, 783–798 (2019).
31. J. Doppler et al., *Nature* **537**, 76–79 (2016).
32. H. Hodaei et al., *Nature* **548**, 187–191 (2017).
33. K. Kawabata, K. Shiozaki, M. Ueda, M. Sato, *Phys. Rev. X* **9**, 041015 (2019).

SUPPLEMENTARY MATERIALS

science.sciencemag.org/content/372/6537/72/suppl/DC1
Materials and Methods
Supplementary Text
Figs. S1 to S5
References (34–38)

Science

Nonlinear tuning of PT symmetry and non-Hermitian topological states

Shiqi Xia, Dimitrios Kaltsas, Daohong Song, Ioannis Komis, Jingjun Xu, Alexander Szameit, Hrvoje Buljan, Konstantinos G. Makris and Zhigang Chen

Nonlinear control of topology

Controlling the topological properties of physical systems provides a platform for developing devices and technology that are robust to defects. Xia *et al.* present a photonic platform in which the underlying dynamics are driven and tuned by the interplay among topology, non-Hermiticity, and nonlinearity (see the Perspective by Roztocki and Morandotti). Using photonic lattices consisting of laser-written waveguides that are continuous ("gain") and sectioned ("loss") and coupled to an interface defect, they demonstrate the nonlinear control of parity-time symmetry and nonlinearity-induced restoration and/or destruction of non-Hermitian topological states. Such concepts are applicable to a broad spectrum of non-Hermitian systems that have intensity-dependent gain or loss and may enable new approaches for light manipulation.
Science, this issue p. 72; see also p. 32

ARTICLE TOOLS	http://science.sciencemag.org/content/372/6537/72
SUPPLEMENTARY MATERIALS	http://science.sciencemag.org/content/suppl/2021/03/31/372.6537.72.DC1
RELATED CONTENT	http://science.sciencemag.org/content/sci/372/6537/32.full
REFERENCES	This article cites 37 articles, 7 of which you can access for free http://science.sciencemag.org/content/372/6537/72#BIBL
PERMISSIONS	http://www.sciencemag.org/help/reprints-and-permissions

Use of this article is subject to the Terms of Service